EUROPEAN ORGANISATION FOR NUCLEAR RESEARCH

CERN-PPE/91-97
18 June 1991

Measurement of Three-Jet Distributions Sensitive to the Gluon Spin in e^+e^- Annihilations at $\sqrt{s} = 91$ GeV

THE OPAL COLLABORATION

Abstract

Three-jet variables constructed from multi-hadronic events produced by Z^0 decays are compared to theoretical calculations assuming a vector gluon or a hypothetical scalar gluon. The data yield conclusive direct evidence for the former case. The distributions of the reduced energy of the second-most energetic jet and of the cosine of the Ellis-Karliner angle are chosen to demonstrate this effect.

(Submitted to Zeitschrift f. Physik C)

G. Alexander[23], J. Allison[16], P.P. Allport[5], K.J. Anderson[9], S. Arcelli[2], J.C. Armitage[6], P. Ashton[16], A. Astbury[a], D. Axen[b], G. Azuelos[18,c], G.A. Bahan[16], J.T.M. Baines[16], A.H. Ball[17], J. Banks[16], G.J. Barker[13], R.J. Barlow[16], J.R. Batley[5], G. Beaudoin[18], A. Beck[23], J. Becker[10], T. Behnke[8], K.W. Bell[20], G. Bella[23], S. Bethke[11], O. Biebel[3], U. Binder[10], I.J. Bloodworth[1], P. Bock[11], H.M. Bosch[11], S. Bougerolle[b], B.B. Brabson[12], H. Breuker[8], R.M. Brown[20], R. Brun[8], A. Buijs[8], H.J. Burckhart[8], P. Capiluppi[2], R.K. Carnegie[6], A.A. Carter[13], J.R. Carter[5], C.Y. Chang[17], D.G. Charlton[8], J.T.M. Chrin[16], P.E.L. Clarke[25], I. Cohen[23], W.J. Collins[5], J.E. Conboy[15], M. Cooper[22], M. Couch[1], M. Coupland[14], M. Cuffiani[2], S. Dado[22], G.M. Dallavalle[2], S. De Jong[8], P. Debu[21], M.M. Deninno[2], A. Dieckmann[11], M. Dittmar[4], M.S. Dixit[7], E. Duchovni[26], G. Duckeck[11], I.P. Duerdoth[16], D.J.P. Dumas[6], G. Eckerlin[11], P.A. Elcombe[5], P.G. Estabrooks[6], E. Etzion[23], F. Fabbri[2], M. Fincke-Keeler[a], H.M. Fischer[3], D.G. Fong[17], C. Fukunaga[24], A. Gaidot[21], O. Ganel[26], J.W. Gary[11], J. Gascon[18], R.F. McGowan[16], N.I. Geddes[20], C. Geich-Gimbel[3], S.W. Gensler[9], F.X. Gentit[21], G. Giacomelli[2], V. Gibson[5], W.R. Gibson[13], J.D. Gillies[20], J. Goldberg[22], M.J. Goodrick[5], W. Gorn[4], C. Grandi[2], E. Gross[26], J. Hagemann[8], G.G. Hanson[12], M. Hansroul[8], C.K. Hargrove[7], P.F. Harrison[13], J. Hart[5], P.M. Hattersley[1], M. Hauschild[8], C.M. Hawkes[8], E. Heflin[4], R.J. Hemingway[6], R.D. Heuer[8], J.C. Hill[5], S.J. Hillier[1], D.A. Hinshaw[18], C. Ho[4], J.D. Hobbs[9], P.R. Hobson[25], D. Hochman[26], B. Holl[8], R.J. Homer[1], S.R. Hou[17], C.P. Howarth[15], R.E. Hughes-Jones[16], R. Humbert[10], P. Igo-Kemenes[11], H. Ihssen[11], D.C. Imrie[25], L. Janissen[6], A. Jawahery[17], P.W. Jeffreys[20], H. Jeremie[18], M. Jimack[2], M. Jobes[1], R.W.L. Jones[13], P. Jovanovic[1], D. Karlen[6], K. Kawagoe[24], T. Kawamoto[24], R.K. Keeler[a], R.G. Kellogg[17], B.W. Kennedy[15], C. Kleinwort[8], D.E. Klem[19], T. Kobayashi[24], T.P. Kokott[3], S. Komamiya[24], L. Köpke[8], R. Kowalewski[6], H. Kreutzmann[3], J. von Krogh[11], J. Kroll[9], M. Kuwano[24], P. Kyberd[13], G.D. Lafferty[16], F. Lamarche[18], W.J. Larson[4], J.G. Layter[4], P. Le Du[21], P. Leblanc[18], A.M. Lee[17], M.H. Lehto[15], D. Lellouch[8], P. Lennert[11], C. Leroy[18], L. Lessard[18], S. Levegrün[3], L. Levinson[26], S.L. Lloyd[13], F.K. Loebinger[16], J.M. Lorah[17], B. Lorazo[18], M.J. Losty[7], X.C. Lou[12], J. Ludwig[10], M. Mannelli[8], S. Marcellini[2], G. Maringer[3], A.J. Martin[13], J.P. Martin[18], T. Mashimo[24], P. Mättig[3], U. Maur[3], T.J. McMahon[1], J.R. McNutt[25], F. Meijers[8], D. Menszner[11], F.S. Merritt[9], H. Mes[7], A. Michelini[8], R.P. Middleton[20], G. Mikenberg[26], J. Mildenberger[6], D.J. Miller[15], C. Milstene[23], R. Mir[12], W. Mohr[10], C. Moisan[18], A. Montanari[2], T. Mori[24], M.W. Moss[16], T. Mouthuy[12], P.G. Murphy[16], B. Nellen[3], H.H. Nguyen[9], M. Nozaki[24], S.W. O'Neale[8,d], B.P. O'Neill[4], F.G. Oakham[7], F. Odorici[2], M. Ogg[6], H.O. Ogren[12], H. Oh[4], C.J. Oram[e], M.J. Oreglia[9], S. Orito[24], J.P. Pansart[21], B. Panzer-Steindel[8], P. Paschievici[26], G.N. Patrick[20], S.J. Pawley[16], P. Pfister[10], J.E. Pilcher[9], J.L. Pinfold[26], D.E. Plane[8], P. Poffenberger[a], B. Poli[2], A. Pouladdej[6], E. Prebys[8], T.W. Pritchard[13], H. Przysiezniak[18], G. Quast[8], M.W. Redmond[9], D.L. Rees[1], K. Riles[4], S.A. Robins[13], D. Robinson[8], A. Rollnik[3], J.M. Roney[9], S. Rossberg[10], A.M. Rossi[2,f], P. Routenburg[6], K. Runge[10], O. Runolfsson[8], D.R. Rust[12], S. Sanghera[6], M. Sasaki[24], A.D. Schaile[10], O. Schaile[10], W. Schappert[6], P. Scharff-Hansen[8], P. Schenk[a], H. von der Schmitt[11], S. Schreiber[3], J. Schwarz[10], W.G. Scott[20], M. Settles[12], B.C. Shen[4], P. Sherwood[15], R. Shypit[b], A. Simon[3], P. Singh[13], G.P. Siroli[2], A. Skuja[17], A.M. Smith[8], T.J. Smith[8], G.A. Snow[17], R. Sobie[g], R.W. Springer[17], M. Sproston[20], K. Stephens[16], H.E. Stier[10], D. Strom[9], H. Takeda[24], T. Takeshita[24], P. Taras[18], S. Tarem[26], P. Teixeira-Dias[11], N.J. Thackray[1], T. Tsukamoto[24], M.F. Turner[5], G. Tysarczyk-Niemeyer[11], D. Van den plas[18], R. Van Kooten[8], G.J. VanDalen[4], G. Vasseur[21], C.J. Virtue[19], A. Wagner[11], C. Wahl[10], J.P. Walker[1], C.P. Ward[5], D.R. Ward[5], P.M. Watkins[1], A.T. Watson[1], N.K. Watson[8], M. Weber[11], S. Weisz[8], P.S. Wells[8], N. Wermes[11], M. Weymann[8], M.A. Whalley[1], G.W. Wilson[21], J.A. Wilson[1], I. Wingerter[8],

V-H. Winterer[10], N.C. Wood[16], S. Wotton[8], T.R. Wyatt[16], R. Yaari[26], Y. Yang[4,h], G. Yekutieli[26], I. Zacharov[8], W. Zeuner[8], G.T. Zorn[17].

[1]School of Physics and Space Research, University of Birmingham, Birmingham, B15 2TT, UK
[2]Dipartimento di Fisica dell' Università di Bologna and INFN, Bologna, 40126, Italy
[3]Physikalisches Institut, Universität Bonn, D-5300 Bonn 1, FRG
[4]Department of Physics, University of California, Riverside, CA 92521 USA
[5]Cavendish Laboratory, Cambridge, CB3 0HE, UK
[6]Carleton University, Dept of Physics, Colonel By Drive, Ottawa, Ontario K1S 5B6, Canada
[7]Centre for Research in Particle Physics, Carleton University, Ottawa, Ontario K1S 5B6, Canada
[8]CERN, European Organisation for Particle Physics, 1211 Geneva 23, Switzerland
[9]Enrico Fermi Institute and Department of Physics, University of Chicago, Chicago Illinois 60637, USA
[10]Fakultät für Physik, Albert Ludwigs Universität, D-7800 Freiburg, FRG
[11]Physikalisches Institut, Universität Heidelberg, Heidelberg, FRG
[12]Indiana University, Dept of Physics, Swain Hall West 117, Bloomington, Indiana 47405, USA
[13]Queen Mary and Westfield College, University of London, London, E1 4NS, UK
[14]Birkbeck College, London, WC1E 7HV, UK
[15]University College London, London, WC1E 6BT, UK
[16]Department of Physics, Schuster Laboratory, The University, Manchester, M13 9PL, UK
[17]Department of Physics and Astronomy, University of Maryland, College Park, Maryland 20742, USA
[18]Laboratoire de Physique Nucléaire, Université de Montréal, Montréal, Quebec, H3C 3J7, Canada
[19]National Research Council of Canada, Herzberg Institute of Astrophysics, Ottawa, Ontario K1A 0R6, Canada
[20]Rutherford Appleton Laboratory, Chilton, Didcot, Oxfordshire, OX11 0QX, UK
[21]DPhPE, CEN Saclay, F-91191 Gif-sur-Yvette, France
[22]Department of Physics, Technion-Israel Institute of Technology, Haifa 32000, Israel
[23]Department of Physics and Astronomy, Tel Aviv University, Tel Aviv 69978, Israel
[24]International Centre for Elementary Particle Physics and Dept of Physics, University of Tokyo, Tokyo 113, and Kobe University, Kobe 657, Japan
[25]Brunel University, Uxbridge, Middlesex, UB8 3PH UK
[26]Nuclear Physics Department, Weizmann Institute of Science, Rehovot, 76100, Israel

[a]University of Victoria, Dept of Physics, P O Box 3055, Victoria BC V8W 3P6, Canada
[b]University of British Columbia, Dept of Physics, 6224 Agriculture Road, Vancouver BC V6T 1Z1, Canada
[c]Also at TRIUMF, Vancouver, Canada V6T 2A3
[d]On leave from Birmingham University, Birmingham B15 2TT, UK
[e]Univ of Victoria, Dept of Physics, P.O. Box 1700, Victoria BC V8W 2Y2, Canada and TRIUMF, Vancouver, Canada V6T 2A3
[f]Present address: Dipartimento di Fisica, Università della Calabria and INFN, 87036 Rende,

Italy
[g]University of British Columbia, Dept of Physics, 6224 Agriculture Road, Vancouver BC V6T 2A6, Canada and IPP, McGill University, High Energy Physics Department, 3600 University Str, Montreal, Quebec H3A 2T8, Canada
[h]On leave from Research Institute for Computer Peripherals, Hangzhou, China

1 Introduction

The theory of quantum chromodynamics (QCD) postulates that the gluon, the gauge boson of the strong force, is self-interacting and has one unit of spin. In the last decade a vast amount of data has been accumulated and has been seen to agree well with this theory. The special properties of hadronic three-jet events resulting from e^+e^- annihilation, where one of the quark-antiquark pairs radiates a gluon, are also well described by QCD theory, either in the form of second order matrix element calculations or parton shower models. Although small differences between data and Monte Carlo remain in the case of $O(\alpha_s^2)$ models, properties dominated by three-jet production are well reproduced [1]. The bulk of the available data, however, does not provide direct evidence for the value of the gluon spin. Several groups at PETRA [2-5] measured three-jet distributions sensitive to the gluon spin, but at energies around 30 GeV the effect was relatively small due to lower statistics and larger hadronization backgrounds, and the conclusions were based solely on first order theory. Other direct evidence for the gluon spin was provided by an analysis of the decay of the Υ resonance into three gluons [6]. The gluon spin affects also the spatial orientation of three-jet events with respect to the beam axis in e^+e^- annihilation [7] [8], but the discriminating power is small. Finally, in $p-\overline{p}$ collisions the angular distribution of jets shows evidence for the gluon spin [9], and the distribution of high p_T leptons is also predicted to depend on it [10].

For measurements of hadronic events in e^+e^- annihilation the higher energies of LEP result in better jet definition, allow for smaller hadronisation corrections and yield higher statistics at the Z^0 resonance. This permits the selection of three-jet distributions with an unambiguous discrimination between scalar and vector gluon theory.

We present here an analysis of about 1.3×10^5 hadronic events obtained with the OPAL detector at LEP during the 1990 data taking run, collected around the Z^0 pole. A similar analysis was recently published by the L3 collaboration [8].

2 Method

Tests for the vector or scalar nature of gluons are based on a comparison of suitable experimental distributions to theoretical expressions, calculated either with the vector or scalar hypothesis. The distributions should be chosen such that the differences between the expected vector and scalar distributions are maximized. The first order cross-sections for the production of three-jet events, because of their simplicity, are well suited to illustrate the method;

To first order the cross-section for producing a three-jet event in e^+ e^- annihilation is proportional to[11]:

$$\frac{d^2\sigma^V(x_1,x_2)}{dx_1dx_2} \sim \frac{x_1^2+x_2^2}{(1-x_1)(1-x_2)} \tag{1}$$

Here $x_i = \frac{2E_i}{E_{cm}}$, $i = 1,2,3$ and $x_1+x_2+x_3 = 2$. E_{cm} is the tot energy of the event. The x_i are the reduced energies of three emitted partons $q, \bar{q}, g$, which hadronize into jets. Since we shall only be interested in the shapes of distributions, we omit here and in the following all constant factors in front of the cross-section expressions.

Equation (1) makes several assumptions:
(i) It applies to massless partons only.
(ii) It assumes that jets labelled 1 and 2 originate from the primary quark and antiquark and that the third jet originates from a gluon, radiated by one of the quarks.
(iii) The gluon is a vector particle.

After fragmentation of the partons into jets consisting of real particles, condition (i) cannot be strictly satisfied, but at at LEP energies the correspondence between jets and the original massless partons is expected to be much improved, compared to previous measurements. One can approximate condition (ii) by ordering jets according to their energy so that $x_1 > x_2 > x_3$. The jet with the lowest energy has then an enhanced probability to correspond to a primary gluon. To account for the finite probability that the more energetic jets 1 and 2 might also originate from a gluon, one has to add to equation (1) symmetric terms obtained by cyclic permutations of the x_i (see appendix eq. (13)).

Equation (1) is usually derived under the assumption that a photon mediates between the initial and final state. On the Z^0 peak it is necessary to account for axial vector as well as vector couplings, but the shape of the x_1, x_2 distribution corresponding to a vector gluon remains unchanged. For a scalar gluon the cross-sections from vector and axial vector couplings are different[12]:

$$\frac{d^2\sigma^S_{(V)}(x_1,x_2)}{dx_1 dx_2} \sim \frac{[(1-x_1)+(1-x_2)]^2}{(1-x_1)(1-x_2)} \tag{2}$$

$$\frac{d^2\sigma^S_{(A)}(x_1,x_2)}{dx_1 dx_2} \sim \frac{[(1-x_1)+(1-x_2)]^2}{(1-x_1)(1-x_2)} - 2(3-x_1-x_2) \tag{3}$$

(for the symmetrized version see appendix eq. (14)). Here and in the following the upper index S or V refers to the type of gluon emitted, while the lower index (V) or (A) refers to the vector and axial-vector type couplings.

If one keeps the x_i ordered and lets x_2 (and therefore also x_1) approach 1, one sees that the vector gluon cross-section σ^V goes to infinity, whereas the scalar cross-sections $\sigma^S_{(V)}$ and $\sigma^S_{(A)}$ tend towards a constant value. This statement remains true even if the other two cyclic terms given in the appendix are included, since the first term of the vector cross-section corresponding to equation (1) dominates if x_1 and x_2 are close to 1. This radically different behaviour between the scalar and vector cross-sections is the basis for the demonstration of the gluon spin.

The limiting factor in the discrimination power of the analysis will be the experimental jet-resolution parameter y_{cut} of the JADE jetfinder, used by us in this analysis to reconstruct and define three-jet events [13]. This parameter y_{cut} represents the square of the minimum invariant pair mass m_{ij} divided by the total visible energy, which all pairs of jets must have in order to be recognized as distinct jets.

$$y_{cut} = (\frac{m_{ij}}{E_{vis}})^2 \quad i,j = 1,2,3, \;\; i \neq j \tag{4}$$

For massless partons in a three-jet configuration the maximum possible value of the x_i is $x_i^{max} = 1 - y_{cut}$. Since x_1 and x_2 close to 1 corresponds to the region of phase-space most sensitive to the gluon spin, a y_{cut} as small as possible is desirable. On the other hand, as x_1 and $x_2 \to 1$, the momentum of the remaining third jet x_3 tends toward zero and will therefore create experimental difficulties of clean detection. Previous investigations of this effect at lower energies [2-5] used y_{cut} values of 0.1 with low discrimination power, whereas with the OPAL detector at the energies

of LEP, an experimental determination of jets down to $y_{cut} = 0.01$ can be made. In a previous publication [14] we have shown that three-jet events can indeed be reliably reconstructed at such a small value of y_{cut}.

Although equation (1) seems at first glance symmetric under exchange of x_1 and x_2, the energy ordering imposed has the effect of forcing x_1 to approach 1 together with x_2 , so that the x_2 distribution as defined here enhances the difference between vector and scalar gluon shapes. We therefore use for our experimental measurement the distribution

$$f^{S,V}(x_2) = \int_{x_2}^{1-y_{cut}} \frac{d^2\sigma^{S,V}(x_1,x_2)}{dx_1 dx_2} dx_1; \quad x_1 > \frac{2}{3}; \quad x_2 < x_1 \tag{5}$$

At lower energies this distribution $f(x_2)$ was not used to test the gluon spin , while two groups, PLUTO [4] and CELLO [3] used the much less sensitive x_1 distribution. Besides the influence of the mathematical pole one can intuitively understand the difference in sensitivity between x_1 and x_2 by realizing that, with the energy ordering imposed here, it is parton 2 which emits most often the gluon and is therefore more affected. The Mark J collaboration [5] used yet another variable, namely the ratio $\frac{x_3^2}{x_1^2+x_2^2}$ which represents the ratio of scalar to vector gluon cross-section.

A different method, also suitable for discriminating between vector and scalar gluons, employs the so-called Ellis-Karliner angle [15], which was used by the TASSO [2] and UA2 collaborations [16]. The idea here is to boost from the laboratory frame to the CM frame of jets 2 and 3, so that they are emitted back-to-back (fig.1). The angle θ between the direction of jet 2 and jet 1 in this frame is called the Ellis-Karliner angle and represents an angular distribution which can be measured. To obtain the cross-sections for this distribution to first order one has to transform the cross-sections of equations (1) and (2) from the $\{x_1, x_2\}$ representation to the $\{x_1, cos\theta_{EK}\}$ representation. Since for massless partons one has:

$$cos\theta_{EK} = \frac{x_2 - x_3}{x_1} \tag{6}$$

one obtains for vector gluons:

$$\frac{d^2\sigma^V(x_1, cos\theta_{EK})}{dx_1 dcos\theta_{EK}} \sim \frac{x_1^2 + [1 + \frac{x_1}{2}(cos\theta_{EK} - 1)]^2}{(1 - x_1)(1 - cos\theta_{EK})} \tag{7}$$

and for scalar gluons (vector coupling term):

$$\frac{d^2\sigma^S_{(V)}(x_1, cos\theta_{EK})}{dx_1 dcos\theta_{EK}} \sim \frac{[1 - x_1 + \frac{x_1}{2}(1 - cos\theta_{EK})]^2}{(1 - x_1)(1 - cos\theta_{EK})} \tag{8}$$

Again the vector gluon cross-section has a pole at $x_1 = 1, cos\theta_{EK} = 1$, whe scalar cross-section does not. Here also a corresponding additional term is needed for axial vector coupling. Taking into account all cyclic permutations of the x_i yields expressions which can again be found in the appendix (equations (16) and (17)). Normalizing these expressions to the value of 1 at $cos\theta_{EK} = 0$ reproduces the formulae cited in the original paper [15] by Ellis and Karliner(see also [22]). The authors of this paper use the thrust T as argument instead of x_1, since T is an event variable which is equal to x_1 in the limit of massless partons.

In analogy to the x_2 case the following one-dimensional distribution $g(cos\theta_{EK})$ is used for comparison with experiment:

$$g^{S,V}(cos\theta_{EK}) = \int_{x_1^{min}}^{1-y_{cut}} \frac{d^2\sigma^{S,V}(x_1, cos\theta_{EK})}{dx_1 dcos\theta_{EK}} dx_1 \tag{9}$$

where x_1^{min} is the minimum value of x_1 allowed by kinematics and energy ordering, for a given $cos\theta_{EK}$.

Another method of calculating these distributions in both the vector and scalar gluon cases is by the Monte Carlo method, which is conveniently done with the JETSET72 Monte-Carlo parton shower simulation program [17], which allows the user to switch between the two gluon hypotheses. The same program contains options to use second order matrix element expressions to generate the $q, \bar{q}, g$ state, but only for the vector gluon hypothesis. For our analysis, JETSET was used extensively to study the sensitivity of the distributions to experimental cuts and model parameters, and to estimate effects of higher order. JETSET72 does not, however, incorporate the correction to the scalar gluon distributions due to the axial vector coupling on the Z^o peak. The author of this program [18] provided us with a modified version which takes this correction into account.

3 Data Selection

The data were recorded with the OPAL detector [20] at the CERN e^+e^- collider LEP. The tracking of charged particles is performed with the central tracking detector, composed of a vertex chamber, a jet chamber and a chamber for precision measurements in the z-direction, all enclosed by a solenoidal magnet coil (z is the coordinate parallel to the beam axis). The principal tracking detector is the jet chamber, which provides up to 159 space-points and close to 100% track finding efficiency for charged tracks in the region $|cos\theta| < 0.92$. Electromagnetic energy deposits ("clusters") are measured with the electromagnetic calorimeter, a detector of lead-glass blocks located in both the barrel and endcap regions, each block of 40x40 mrad^2 cross section, for a total detector solid angle coverage of 98% of 4π.

The trigger and online event selection for hadronic events are described in [21]. Additional criteria were applied for this analysis to reduce the small level of background and to obtain well contained events. Charged tracks were accepted if they originated from within 5 cm of the interaction point in the direction perpendicular to the beam axis. The minimum transverse momentum was set at 150 MeV/c, the absolute value of the cosine of the angle to the beam direction had to be less than .93 and the track was required to have at least 20 measured space-points. Electromagnetic clusters were accepted if they deposited at least 0.2 GeV in the electromagnetic calorimeter and if at least two contiguous lead glass blocks were included in the cluster. Noisy blocks were eliminated from the analysis. Hadronic events were required to contain at least 5 charged tracks and a polar angle for the thrust direction, defined using the accepted charged tracks and electromagnetic clusters, in the range $|cos(\theta_{thrust})| < 0.90$. Events were also rejected if the visible energy was less than 40% of the CM energy, or if the total momentum imbalance or the longitudinal momentum imbalance along the beam direction exceeded 40% of the CM energy. Finally the jet masses of the events, considered as two jet events for this purpose, were required to be greater than 2 GeV. From a data sample of 127 191

events at $\sqrt{s} = 88.3 - 95.0$ GeV used for this analysis, 111 049 events remained after all cuts. Using a y_{cut} of 0.01, 56 098 three-jet events were obtained for further analysis.

4 Measurements of x_2 and Ellis-Karliner Distributions

In order to compare the present measurements with theoretical calculations at the parton level, one must unfold the measured $f(x_2)$ and $g(cos\theta_{EK})$ distributions for detector acceptance, resolution, initial-state photon radiation and fragmentation. The fact that QCD parton shower models with different mechanisms for fragmentation describe the detailed features of hadronic event structure from $\sqrt{s} = 30$ to 91 GeV using energy independent parameters [1], implies that the size of the fragmentation corrections may be estimated reliably. The unfolding procedure is based on a detailed simulation of the OPAL detector and is described in [1]. It leads to bin-by-bin corrections defined, for $f(x_2)$ and $g(cos\theta_{EK})$, by

$$(f(x_2)^{data}_{parton})_i = \left[\frac{(f(x_2)^{M.C.}_{parton})_i}{(f(x_2)^{M.C.}_{det.})_i}\right] \cdot (f(x_2)^{data}_{meas.})_i \quad ; \quad i = \text{ bin index}, \tag{10}$$

where $f(x_2)^{M.C.}_{parton}$ refers to Monte Carlo events at the parton level, without initial-state radiation, fragmentation or detector simulation, while $f(x_2)^{M.C.}_{det.}$ refers to Monte Carlo events at the hadron level with initial-state radiation and detector simulation, which have been passed through the same reconstruction and selection algorithms as the data. The distributions $f(x_2)^{data}_{meas.}$ and $f(x_2)^{data}_{parton}$ are the directly measured distributions and the measured distributions unfolded to the parton level, respectively. For the measurements charged tracks and electromagnetic clusters not associated to tracks [1] were used.

In our analysis we evaluated x_2 using the angular definition:

$$x_2 = \frac{2sin\theta_{31}}{sin\theta_{12} + sin\theta_{23} + sin\theta_{31}} \tag{11}$$

Here θ_{31} is the angle between the two jets opposite to x_2. It was found that with this definition of x_2 the corrections between parton and hadron levels were smaller than with other definitions. The same correction procedure is applied to $g(cos\theta_{EK})$, where θ_{EK} is the Ellis-Karliner angle. Following [15], this angle was evaluated using the thrust T to boost jets 2 and 3 into their CM system.

The ratios defined by the terms in square brackets in (10) were obtained from the JETSET parton shower model [17] with parameter values adjusted to describe global event shapes measured by OPAL [1]. The JETSET parton shower is a model based on the leading log approximation, where the shower is terminated at a virtual parton mass of $Q_0 = 1GeV$. That this model plus detector simulation provides already a reasonably good description of the measured distributions before the corrections are applied, can be seen in column 3 of tables 1 and 2, where the ratios DATA/MC, which is the ratio of the measured distribution to the Monte Carlo one with full detector simulation, are listed. One can see that these ratios are never far from unity, although there is a systematic trend for the data to be more peaked than the simulation for x_2 and $cos\theta_{EK}$ close to 1. The correction factors of eq.(10) are listed in column 5 of tables 1 and 2. Systematic errors due to imperfections in the simulation of the detector or in the event reconstruction were

[1] A cluster in the electromagnetic barrel was not considered for association to a track if it fell outside a region delimited by $\Delta\theta = 150$ mr and $\Delta\phi = 80$mr. In the electromagnetic endcap 50 mr for both $\Delta\theta$ and $\Delta\phi$ was used.

estimated by taking the difference between the unfolded distributions derived from the tracking chambers alone to those derived from the tracking chambers plus calorimeters, and similarly for distributions derived from electromagnetic clusters alone. The differences at the parton level between the JETSET72 and another shower model, HERWIG43 [19], were taken as an indication of theoretical uncertainties and included in the systematic error. The various contributions to the systematic errors were added in quadrature.
In figures 2 and 3 are shown the measured x_2 and Ellis-Karliner distributions, $f(x_2)$ and $g(cos\theta_{EK})$, unfolded to the parton level using JETSET with the parameter values discussed above. The numerical values are given in the second column of tables 1 and 2 respectively. All quoted values are normalized to the total number of extracted 3 jet events. In column 4 of tables 1 and 2 the factors

$$\left[\frac{(f(x_2)^{M.C.}_{hadron})_i}{(f(x_2)^{M.C.}_{parton})_i}\right] \quad ; \quad i = \text{ bin index} \tag{12}$$

are given(similarly for $g(cos\theta_{EK})$), which show the importance of fragmentation corrections (column 2 times column 4 yields the measured distributions corrected to the hadron level).

5 Results and Discussion

The essential result of this work is contained in figs.2 and 3, where data are compared with several theoretical curves for both the $f(x_2)$ and $g(cos\theta_{EK})$ distributions: the predictions for a scalar gluon [2] or a vector gluon model using the JETSET parton shower, and first order analytical calculations based on formulae (1) and (2), for the vector and scalar gluon cases. A second order matrix element calculation in the vector gluon hypothesis, using the default parameters of the JETSET package, is also shown.
The spectra are normalized with respect to each other, so that this comparison is based on shape only. [3]

Both the analytical first order and the shower model scalar gluon curves are manifestly incompatible with the data, while the curves based on the normal vector gluon model fit the data overall quite well. Some differences between the various models and the data remain: in the case of the Ellis-Karliner distribution the parton shower gives the better description, while the second order matrix element calculation gives a better fit to the experimental x_2 distribution. It should be pointed out that the definition of the quantities x_2 and $cos\theta_{EK}$ is not unique: e.g. x_2 could have been calculated using $x_2{=}2E_2/E_{vis}$ instead of equation (11), and $cos\theta_{EK}$ could have been evaluated using equation (6) instead of the boost method employed in this analysis. These different methods yield identical predictions in leading order for massless partons only, while for massive partons or jets the shapes of the distributions and the description of the experimental data are subject to slight variations.

Irrespective of the differences between the various models it is clear, however, that the data unambiguously favor the vector gluon hypothesis, due to the large differences between the vector and scalar distributions in figures 2 and 3.

We verified that increasing y_{cut} to larger values causes the peak observed in the data for x_2 or $cos\theta_{EK} \approx 1$ to decre in height, in accordance with the expectations from vector models. The

[2]The distributions shown were found to be insensitive to the choice of the JETSET parameters $c_{g\to gg}$ and $c_{g\to qq}$.

[3]The discontinuity in the slope of the analytical x_2 distribution at $x_2 = \frac{2}{3}$ is caused by the ordering of the x_i, which limits x_1 to values above $\frac{2}{3}$

vector gluon hypothesis remains strongly favored even for these larger y_{cut} values. The peak of the first order vector calculations is at slightly higher x_2 and $cos\theta_{EK}$ values than the data. A better fit is obtained with models which include higher order corrections as seen from the curves corresponding to the parton shower and second order matrix element models. The prominence of this pole in the data for x_2 and $cos\theta_{EK}$ close to one remains a striking feature of both first and higher order models.

The conclusion, that the observed distributions are incompatible with the scalar gluon hypothesis, can also be based quantitatively on a fit of the experimental data with a mixture of scalar and vector gluon shapes. This leads to a determination of the possible fraction of events with a scalar shape that could be compatible with our data. The results again vary for the different theories and the two measured data sets. From the analysis we present here, the largest possible value of the fraction of scalar events is obtained using the experimental x_2 distribution and as vector gluon theory the second order matrix calculation. For the scalar gluon case a second order matrix calculation not being available, the parton shower was used instead. For this case one then obtains that the possible fraction of events with a scalar spectrum shape is lower than 2.4% at the one standard deviation level.

One final remark: The measured distributions are very convincing visual evidence for a gluon of spin one. They have been derived by studying the shape of three-jet events in the hadronic event sample. Actually the fraction of those three-jet events in the hadronic data sample, given by the ratio R_3, is already evidence of the vector nature of the gluon, since both shower models and first order calculations predict a reduction of R_3 by an order of magnitude in going from a vector to a scalar model (keeping all else, in particular α_s, constant), again totally incompatible with experiment.

6 Conclusions

The general shapes of the measured distributions of the reduced energy of the second-most energetic jet and of the cosine of the Ellis-Karliner angle are reproduced by Monte-Carlo shower and second order matrix element models, and are also approximately reproduced by first order analytical matrix calculations. Due to the low value of the jet resolution parameter y_{cut} used, they provide good evidence for the pole structure of the three-jet cross-section corresponding to a gluon spin equal to 1. They are in strong disagreement with calculations assuming a gluon of spin zero.
The possible fraction of hypothetical events with a scalar shape contained in the data is lower than 2.4% at the level of one standard deviation.

Acknowledgments

We thank G.Belanger, Z.Fodor and J.Ellis for helpful discussions concerning the first order formulae. We are indebted to P.Zerwas for calculating the correction term for scalar 3-jet distributions in the case of axial vector coupling and to T.Sjöstrand for incorporating this term into the JETSET package.

It is a pleasure to thank the SL Division for the efficient operation of the LEP accelerator, the precise information on the absolute energy, and their continuing close cooperation with our experimental group. In addition to the support staff at our own institutions we are pleased to acknowledge the following :
Department of Energy, USA
National Science Foundation, USA
Science and Engineering Research Council, UK
Natural Sciences and Engineering Research Council,Canada
Israeli Ministry of Science
Minerva Gesellschaft
The Japanese Ministry of Education, Science and Culture (the Monbusho) and a grant under the Monbusho International Science Research Program.
American Israeli Bi-national Science Foundation.
Direction des Sciences de la Matière du Commissariat à l'Energie Atomique, France.
The Bundesministerium für Forschung und Technologie, FRG.
and The A.P. Sloan Foundation.

Appendix

Equations (1),(2),(7) and (8) apply to the case where the gluon is particle number three. To include the probability of the gluon being particle number one or two, one has to sum over all cyclic permutations of these formulae. The resulting expressions are:

$$\frac{d^2\sigma^V(x_1,x_2)}{dx_1dx_2} \sim \frac{x_1^3+x_2^3+x_3^3}{(1-x_1)(1-x_2)(1-x_3)} \tag{13}$$

$$\begin{aligned}\frac{d^2\sigma^S(x_1,x_2)}{dx_1dx_2} &\sim A\cdot C_v^2+(A+B)\cdot C_a^2 \\ &\sim A+B\cdot\frac{C_a^2}{C_v^2+C_a^2}\end{aligned} \tag{14}$$

where

$$\begin{aligned}A &= \frac{x_1^2(1-x_1)+x_2^2(1-x_2)+x_3^2(1-x_3)}{(1-x_1)(1-x_2)(1-x_3)} \\ B &= -10\end{aligned} \tag{15}$$

The terms A and B are derived from cyclic permutations of the vector coupling term in eq. (2), and of the correction term $-2(1+x_3)$ for the axial coupling (see eq. 3) respectively. The correction factor $B\frac{C_a^2}{C_v^2+C_a^2}$ is equal to 7.45. Here the standard model vector and axial-vector couplings C_v^2 and C_a^2 for the u,d,s,c,b quarks were assumed and a value of $sin^2\theta_W$ of .233 was used.

The equivalent symmetrized expressions in terms of the Ellis-Karliner angle are:

$$\frac{d^2\sigma^V(x_1,cos\theta_{EK})}{dx_1dcos\theta_{EK}} \sim \frac{4x_1^3+(2-x_1)^3+3x_1^2(2-x_1)cos^2\theta_{EK}}{2x_1(1-x_1)(1-cos^2\theta_{EK})} \tag{16}$$

$$\frac{d^2\sigma^S(x_1,cos\theta_{EK})}{dx_1dcos\theta_{EK}} \sim \frac{4-3x_1^2+x_1(3x_1-4)cos^2\theta_{EK}}{2(1-x_1)(1-cos^2\theta_{EK})} - 7.45\frac{x_1}{2} \tag{17}$$

The correction factor in this case is $7.45\frac{x_1}{2}$, where $\frac{x_1}{2}$ is the jacobian of the transformation from the x_1, x_2 system to the $x_1, cos\theta_{EK}$ system.

References

[1] OPAL Collaboration, M.Z. Akrawy et al., Z. Phys. C47 (1990), 505

[2] TASSO Collaboration, R.Brandelik et al., Phys.Lett. 97B (1980) 453
S.Wu, Physics Reports 107 (1984) p.162

[3] CELLO Collaboration, H.J.Behrend et al., Phys. Lett. 110B (1982) 329
S.Wu, Physics Reports 107 (1984) p.163

[4] PLUTO Collaboration, Ch.Berger et al., Phys. Lett. 97B (1980) 459
S.Wu, Physics Reports 107 (1984) p.163

[5] Mark J Collaboration, J.D.Burger et al., proceedings of the 21^{st} International Conference on High Energy Physics, Paris 1982, Journal de Physique 43, C3-C6

[6] K.Koller and H.Krasemann, Phys. Lett. 88B (1979) 119

[7] P.W.Johnson and W.Tung, Z. Phys. C13 (1982) 87
D.H.Schiller and G.Zech, Physica Scripta 26 (1982) 273

[8] L3 preprint No.30, CERN-PPE, May 1991

[9] UA1 Collaboration, G. Arnison et al., Phys. Lett. 136B (1984) 294
UA2 Collaboration, P. Bagnaia et al., Phys. Lett. 144B (1984) 284

[10] N.Arteaga-Romero, A.Nicolaidis and J.Silva, Phys. Rev. Lett. 52 (1984) 172

[11] G.Kramer, Springer Tracts in Modern Physics, vol. 102 (1984) p.39

[12] E.Laermann, K.H.Streng and P.M.Zerwas, Z. Physik C3 (1980) 289
E.Laermann, K.H.Streng and P.M.Zerwas, Erratum to be published in Z. Phys.
P. Zerwas, private communication

[13] JADE Collaboration, S.Bethke et al., Phys. Lett. 213B (1988) 235

[14] OPAL Collaboration, M.Z. Akrawy et al., Phys. Lett. 235B (1990) 389

[15] J.Ellis and I.Karliner, Nucl. Phys. B148 (1979) 141
J.Ellis, I.Karliner and W.J.Stirling, Phys. Lett. 217B (1989) 363

[16] UA2 Collaboration, J.A.Appel et al., Z. Physik C30 (1986) 341

[17] T. Sjöstrand, Comp. Phys. Comm. 39 (1986) 347;
T. Sjöstrand and M. Bengtsson, Comp. Phys. Comm. 43 (1987) 367

[18] T. Sjöstrand, private communication

[19] G.Marchesini and B.R. Webber, Nucl. Phys. B310 (1988) 461

[20] OPAL collaboration, K. Ahmet et al., CERN-PPE/90-114,
Submitted to Nucl. Instr. and Meth.

[21] M.Arignon et al., CERN-PPE/91-32 (1991)
submitted to Nucl. Instr. and Meth.
OPAL Collaboration, M.Z.Akrawy et al., Phys. Lett. 231 (1989) 530

[22] I.J.R. Aitchison and A.J.G. Hey: " Gauge Theories in Particle Physics", Adam Hilger 1989, p. 316

Figure Captions

Figure 1:
Definition of the Ellis-Karliner angle

Figure 2:
Distributions of the reduced energy x_2 of the second jet at $y_{cut} = .01$;

i) Experimental distributions corrected to the parton level (circles);
ii) The predictions of the JETSET parton shower model for vector gluons (hatched area);
iii) The predictions of the JETSET parton shower model for scalar gluons (dashed histogram);
iv) The predictions of the JETSET second order matrix element model for vector gluons(solid histogram);
v) The predictions of the first order analytical calculations for vector and scalar gluons(solid and dashed curves).

The scalar models contain a correction term to account for axial vector coupling on the Z^0 peak.
All curves are normalized with respect to each other so as to have the same integral.

Figure 3:
Distributions of the Ellis-Karliner angle at $y_{cut} = .01$;

i) Experimental distributions corrected to the parton level (circles);
ii) The predictions of the JETSET parton shower model for vector gluons (hatched area);
iii) The predictions of the JETSET parton shower model for scalar gluons (dashed histogram);
iv) The predictions of the JETSET second order matrix element model for vector gluons(solid histogram);
v) The predictions of the first order analytical calculations for vector and scalar gluons(solid and dashed curves).

The scalar models contain a correction term to account for axial vector coupling on the Z^0 peak.
All curves are normalized with respect to each other so as to have the same integral.

x_2 (bin center)	data (parton level)	ratio DATA/MC	corr.factor fragmentation	corr.factor PARTONS/MC
0.4925	0.009 $\pm$.003 $\pm$.005	1.146 $\pm$.343	1.017 $\pm$.199	1.450 $\pm$.324
0.5275	0.276$\pm$.012 $\pm$.036	0.831 $\pm$.036	0.774 $\pm$.027	1.040 $\pm$.031
0.5625	0.468 $\pm$.017 $\pm$.047	0.876 $\pm$.032	0.892 $\pm$.023	1.209 $\pm$.031
0.5975	0.511 $\pm$.017 $\pm$.079	0.824 $\pm$.027	0.909 $\pm$.022	1.138 $\pm$.026
0.6325	0.589 $\pm$.018 $\pm$.091	0.849 $\pm$.027	0.895 $\pm$.020	1.154 $\pm$.025
0.6675	0.692 $\pm$.020 $\pm$.115	0.890 $\pm$.026	0.882 $\pm$.019	1.153 $\pm$.024
0.7025	0.735 $\pm$.021 $\pm$ .103	0.895 $\pm$.025	0.904 $\pm$.019	1.097 $\pm$.021
0.7325	0.778 $\pm$.021 $\pm$ .149	0.870 $\pm$.023	0.905 $\pm$.018	1.100 $\pm$.021
0.7725	0.963 $\pm$.024 $\pm$ .101	0.967 $\pm$.024	0.888 $\pm$.017	1.138 $\pm$.021
0.9075	1.144 $\pm$.027 $\pm$ .093	1.026 $\pm$.024	0.921 $\pm$.016	1.145 $\pm$.020
0.8425	1.336 $\pm$.029 $\pm$ .031	1.035 $\pm$.022	0.915 $\pm$.015	1.084 $\pm$.017
0.8778	1.594 $\pm$.031 $\pm$ .105	1.036 $\pm$.020	0.936 $\pm$.014	1.032 $\pm$.014
0.9125	2.025 $\pm$.034 $\pm$ .073	1.095 $\pm$.018	0.952 $\pm$.013	0.980 $\pm$.012
0.9475	2.441 $\pm$.036 $\pm$ .132	1.105 $\pm$.016	1.054 $\pm$.012	0.881 $\pm$.010
0.9825	1.439 $\pm$.024 $\pm$ .108	1.012 $\pm$.016	1.764 $\pm$.020	0.700 $\pm$.008

Table 1: Results of the measurement of the distribution $f(x_2)$ at $y_{cut} = .01$.
1^{st} column: x_2 values at bin center.
2^{nd} column: Corrected data at the parton level with statistical and systematic errors. The systematic errors include the differences between JETSET and HERWIG Monte Carlo calculations as well as differences between analyses using charged tracks plus electromagnetic clusters and charged tracks or electromagnetic clusters alone.
3^{rd} column: Ratios (Data)/(Detector Level MC) with statistical errors.
4^{th} column: Correction factors for fragmentation with statistical errors.
5^{th} column: Correction factors (partons)/(Detector Level MC) with statistical errors.

$cos\theta_{EK}$ (bin center)	data (parton level)	ratio DATA/MC	corr.factor fragmentation	corr.factor PARTONS/MC
0.05	0.373 $\pm$.012 $\pm$ .034	0.896 $\pm$.028	0.803 $\pm$.020	1.094 $\pm$.025
0.15	0.442 $\pm$.014 $\pm$ .040	0.896 $\pm$.027	0.773 $\pm$.018	1.202 $\pm$.026
0.25	0.480 $\pm$.014 $\pm$ .070	0.858 $\pm$.025	0.807 $\pm$.018	1.177 $\pm$.024
0.35	0.571 $\pm$.015 $\pm$ .098	0.900 $\pm$.024	0.777 $\pm$.016	1.157 $\pm$.022
0.45	0.686 $\pm$.017 $\pm$ .067	0.944 $\pm$.022	0.848 $\pm$.016	1.106 $\pm$.019
0.55	0.825 $\pm$.018 $\pm$ .084	0.957 $\pm$.020	0.890 $\pm$.015	1.075 $\pm$.017
0.65	1.072 $\pm$.020 $\pm$ .042	1.000 $\pm$.019	0.916 $\pm$.014	1.029 $\pm$.014
0.75	1.461 $\pm$.024 $\pm$ .026	1.047 $\pm$.017	0.940 $\pm$.012	1.037 $\pm$.013
0.85	2.035 $\pm$.029 $\pm$ .089	1.055 $\pm$.015	0.971 $\pm$.010	1.062 $\pm$.011
0.95	2.054 $\pm$.025 $\pm$ .245	1.044 $\pm$.012	1.480 $\pm$.013	0.762 $\pm$.007

Table 2: Results of the measurement of the distribution $g(cos\theta_{EK})$ at $y_{cut} = .01$.
1^{st} column: $cos\theta_{EK}$ values at bin center.
2^{nd} column: Corrected data at the parton level with statistical and systematic errors. The systematic errors include the differences between JETSET and HERWIG Monte Carlo calculations as well as differences between analyses using charged tracks plus electromagnetic clusters and charged tracks or electromagnetic clusters alone.
3^{rd} column: Ratios (Data)/(Detector Level MC) with statistical errors.
4^{th} column: Correction factors for fragmentation with statistical errors.
5^{th} column: Correction factors (Partons)/(Detector Level MC) with statistical errors.

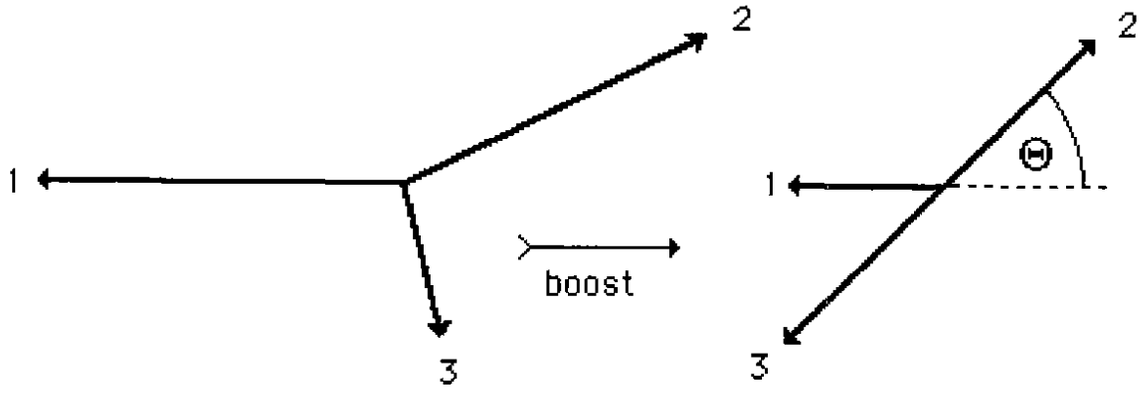

Fig.1

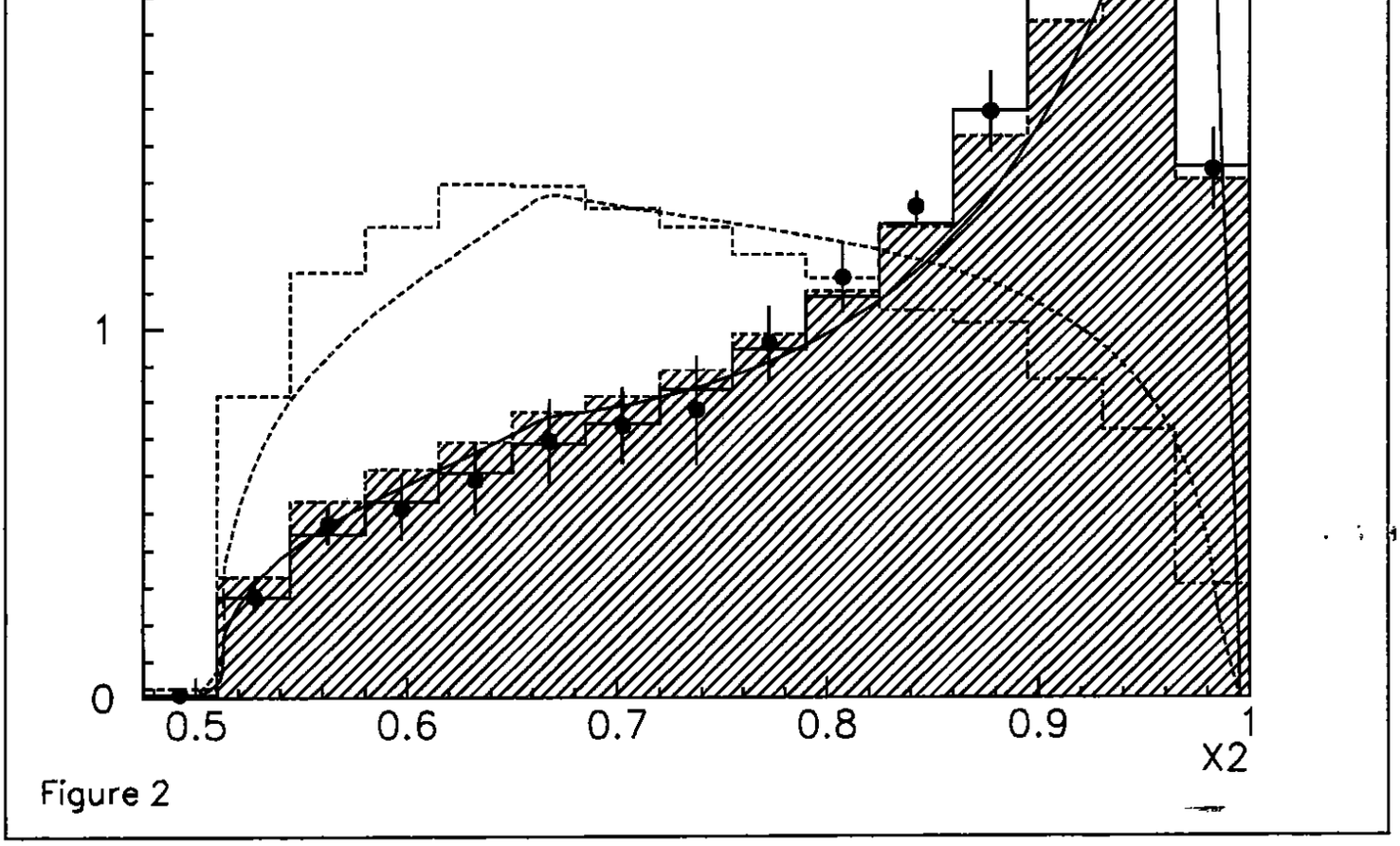
X2 distribution, Ycut=.01
(1/N)(dN/dX2)
Corrected data
Hatched area: JETSET PS vector gluon
Dashed histogram: JETSET PS scalar gluon
Solid histogram: JETSET 2nd ord. ME vector
Solid line: 1st order vector
Dashed line: 1st order scalar
OPAL
0
1
2
3
0.5
0.6
0.7
0.8
0.9
1
X2

Figure 2

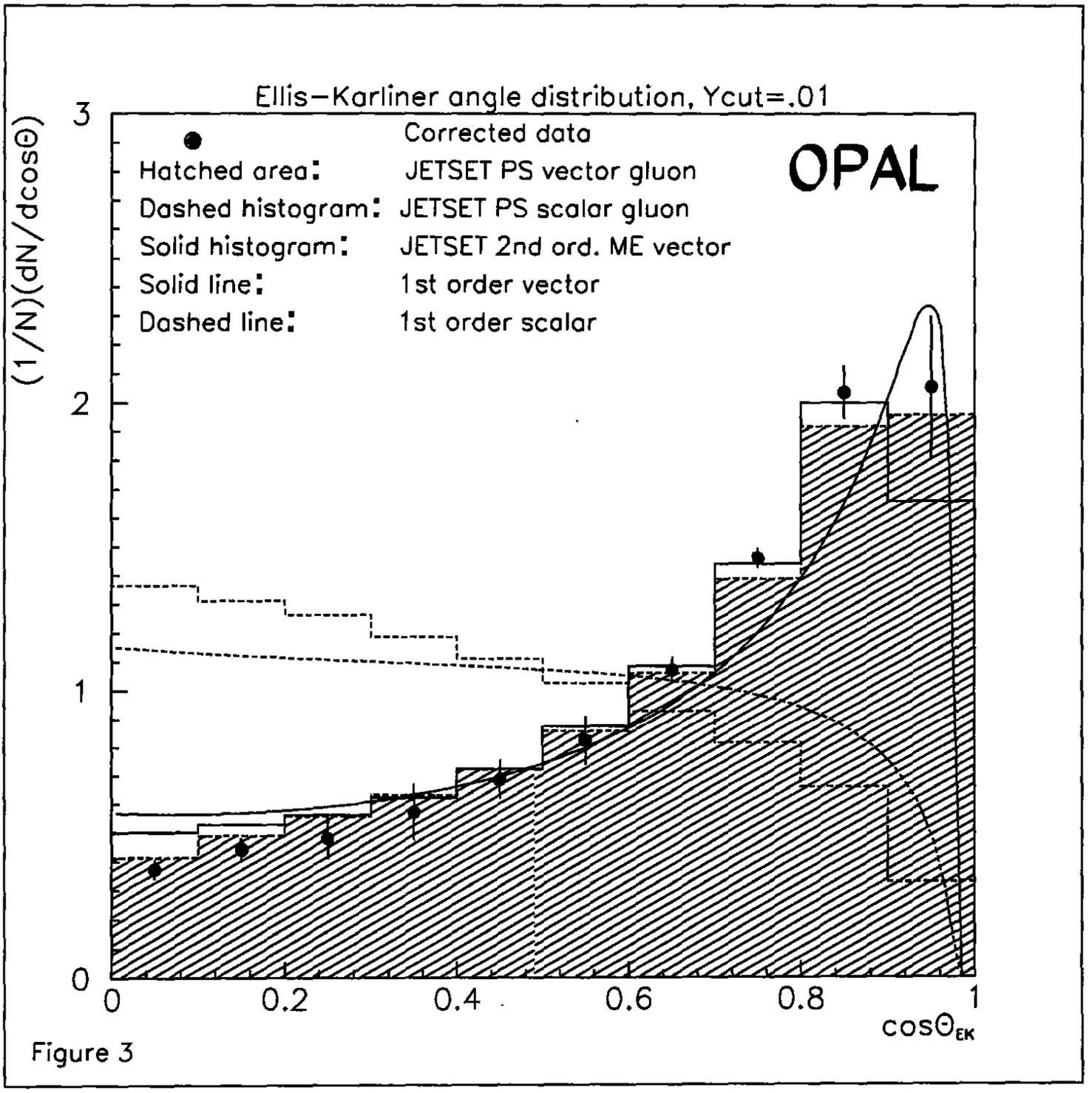
Ellis–Karliner angle distribution, Ycut=.01
(1/N)(dN/dcosΘ)
Corrected data
Hatched area: JETSET PS vector gluon
Dashed histogram: JETSET PS scalar gluon
Solid histogram: JETSET 2nd ord. ME vector
Solid line: 1st order vector
Dashed line: 1st order scalar
OPAL
0
1
2
3
0
0.2
0.4
0.6
0.8
1
cosΘEK

Figure 3